Wind-Blown Bubbles around Evolved Stars

S. Jane Arthur

Centro de Radioastronomía y Astrofísica, UNAM, Campus Morelia, Apartado Postal 3-72, 58090 Morelia, Michoacán, México `j.arthur@astrosmo.unam.mx`.

Most stars will experience episodes of substantial mass loss at some point in their lives. For very massive stars, mass loss dominates their evolution, although the mass loss rates are not known exactly, particularly once the star has left the main sequence. Direct observations of the stellar winds of massive stars can give information on the current mass-loss rates, while studies of the ring nebulae and HI shells that surround many Wolf-Rayet (WR) and luminous blue variable (LBV) stars provide information on the previous mass-loss history. The evolution of the most massive stars, $M > 25 M_\odot$, essentially follows the sequence O star $\rightarrow$ LBV or red supergiant (RSG) $\rightarrow$ WR star $\rightarrow$ supernova. For stars of mass less than $\sim 25 M_\odot$ there is no final WR stage. During the main sequence and WR stages, the mass loss takes the form of highly supersonic stellar winds, which blow bubbles in the interstellar and circumstellar medium. In this way, the mechanical luminosity of the stellar wind is converted into kinetic energy of the swept-up ambient material, which is important for the dynamics of the interstellar medium. In this article, analytic and numerical models are used to describe the hydrodynamics and energetics of wind-blown bubbles. A brief review of observations of bubbles is given, and the degree to which theory is supported by observations is discussed.

1 Classical wind-blown bubbles

The effect that a stellar wind has on its surroundings can be dramatic. A massive star will first have formed an H II region around itself, and so the stellar wind interacts with this ionized gas. A fast (typically 2000 km s^{-1}) stellar wind is hypersonic with respect to the ambient medium (sound speed $\sim$10 km s^{-1} in photoionized gas) and so a two-shock flow pattern forms: one shock sweeps up the ambient medium, accelerating, compressing and heating it, while the other shock decelerates the stellar wind itself, heating and compressing it (Pikel'ner, 1968; Dyson & de Vries, 1972; Avedisova, 1972). The
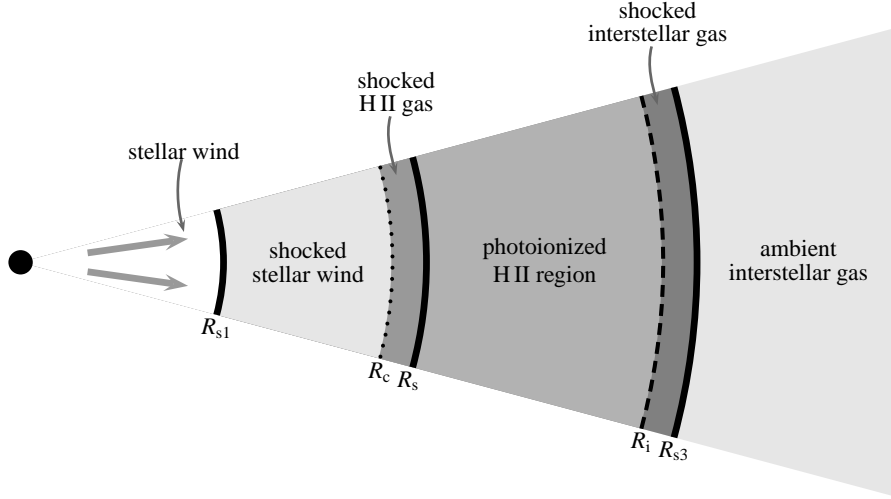
Fig. 1. Schematic of the different regions of a wind-blown bubble around a massive star. R_{s1} is the stellar wind shock, R_s is the shock set up in the ambient medium, and R_{s3} is the isothermal shock sent out ahead of the ionization front that borders the H II region, while R_c is the contact discontinuity separating shocked stellar wind material from swept-up ambient medium and R_i marks the ionization front, separating neutral and ionized gas.

basic scenario is shown in Figure 1. In most treatments, the photionized region and the neutral shell beyond the stellar wind bubble are not discussed separately, and it is assumed that the shock R_s expands into a fully ionized ambient medium.

Conditions behind the ambient medium shock, R_s, favour rapid cooling of the swept-up shell of material, which occurs once the shock velocity falls below 200 km s^{-1}, so that this region becomes thin and dense (Falle, 1975). The shocked stellar wind, however, can have temperature $> 10^7$ K and thus does not cool efficiently. A hot, very low density bubble of shocked stellar wind forms, which pushes the cold, swept-up shell like a piston. Since the hot shocked wind remains adiabatic, this is known as an "energy-driven" flow.

If the ambient medium has a radial power-law density distribution $\rho(r) = \rho_0 r^\beta$, and R_s and $V_s \equiv \dot{R}_s$, are the radius and velocity of the bubble-driven shock, respectively, then the expansion law for the hot bubble can be found by considering momentum and energy conservation, with the assumption that $R_s = R_c$, i.e., that the region of swept-up ambient medium is thin (Dyson, 1984, 1989). The momentum and energy equations are

$$\frac{d}{dt}\left(\frac{4\pi}{3+\beta}\rho_0 R_s^{3+\beta}V_s\right) = 4\pi R^2 P \tag{1}$$

$$\frac{d}{dt}\left(\frac{4\pi}{3}R_s^3\frac{P}{\gamma-1}\right) = \dot{E}_w - 4\pi R_s^2 P V_s \qquad (2)$$

where P is the thermal pressure in the hot bubble, giving as solution

$$R_s = \phi^{1/(5+\beta)}\left(\frac{2\dot{E}_w}{\rho_0}\right)^{1/(5+\beta)}t^{3/(5+\beta)} \ , \qquad (3)$$

$$V_s = \left(\frac{3}{5+\beta}\right)\frac{R_s}{t} \ , \qquad (4)$$

with

$$\phi = \frac{(3+\beta)(5+\beta)^3}{12\pi(11+\beta)(7+2\beta)} \ . \qquad (5)$$

Here, the stellar wind mechanical luminosity, $\dot{E}_w \equiv \frac{1}{2}\dot{M}_w V_w$, is taken to be constant, and $\dot{M}_w$, V_w are the stellar wind mass-loss rate and velocity, respectively. A time-varying stellar wind mechanical luminosity was considered by García-Segura & Mac Low (1995a). The case $\beta = 0$ (i.e., constant density ambient medium) returns the well-known formulae of the thin shell approximation for stellar wind bubble evolution (Weaver et al., 1977). The case $\beta = -2$ would represent a wind bubble expanding into the density distribution left by the wind of a previous evolutionary stage of the star.

"Momentum-driven" flows occur when the shocked wind cools in a time much less than the dynamical timescale. The swept-up shell of ambient material is driven by the momentum of the wind rather than by the pressure of the shocked wind. The expansion law can be found by considering momentum conservation.

$$\frac{d}{dt}\left(\frac{4\pi}{3}\rho_0 R_s^{3+\beta}V_s\right) = \dot{M}_w V_w \ . \qquad (6)$$

For constant wind momentum, $\dot{M}_w V_w$, the radius and velocity of the outer shock are given by (Dyson, 1984, 1989)

$$R_s = \chi^{1/(4+\beta)}\left(\frac{\dot{M}_w V_w}{\rho_0}\right)^{1/(4+\beta)}t^{2/(4+\beta)} \ , \qquad (7)$$

$$V_s = \left(\frac{2}{4+\beta}\right)\frac{R_s}{t} \ , \qquad (8)$$

with

$$\chi = \frac{(3+\beta)(4+\beta)}{8\pi} \ . \qquad (9)$$

A flow can be defined as energy or momentum driven by the thermal behaviour of the shocked stellar wind at a time, t_0, when the wind has swept up its own mass of ambient material. If the shocked wind can cool by this time then the flow will be momentum driven, otherwise it is energy driven.

The cooling time in the shocked stellar wind can be estimated using Kahn's approximation to the cooling rate, $L = AT^{-1/2}n^2$ erg cm^{-3} s^{-1}, in the temperature range $10^5 < T < 2 \times 10^7$ K (Kahn, 1976), where $A = 1.3 \times 10^{-19}$ is a constant and n and T are the number density and temperature, respectively, in the shocked gas. The cooling time is thus

$$t_{\text{cool}} = \frac{p}{(\gamma - 1)L} \approx 4 \times 10^{-35} \frac{V_w^3}{\rho_R} \ , \tag{10}$$

where a mean nucleon mass of $m_p = 2 \times 10^{-24}$ g has been used and it is assumed that the gas is fully ionized.[1] For a momentum-driven flow, $\rho_R = \dot{M}_w V_w / 4\pi R_{s1}^2$, where R_{s1} is assumed to be the same as R_s (see Eq. 7), since both the shocked wind and shocked swept-up ambient medium shells are thin in this approximation. Hence

$$t_{\text{cool}} \simeq 1 \times 10^{-33} \chi^{2/(4+\beta)} \dot{M}_w^{-(2+\beta)/(4+\beta)} V_w^{(18+4\beta)/(4+\beta)} \rho_0^{-2/(4+\beta)} t^{2/(4+\beta)} \tag{11}$$

in this case.

When the flow is energy driven, the interior pressure of the hot bubble, P_b, is uniform and can be found by substituting equations 3 and 4 into equation 1. The density in the hot, shocked stellar wind is $n = P_b/2kT$, where T is the post-shock temperature, which depends only on the stellar wind velocity. In this case, therefore, the cooling time is given by

$$t_{\text{cool}} \simeq 2 \times 10^{-35} \xi \dot{M}_w^{-(2+\beta)/(5+\beta)} V_w^{3(7+\beta)/(5+\beta)} \rho_0^{-3/(5+\beta)} t^{(4-\beta)/(5+\beta)} \ , \tag{12}$$

where

$$\xi = \frac{(5+\beta)^2(3+\beta)}{(7+2\beta)\phi^{2+\beta}} \ . \tag{13}$$

The ratio of the cooling time to the dynamical time thus varies as $t^{-\beta/(4+\beta)}$ for a momentum-driven flow and $t^{-(1+2\beta)/(5+\beta)}$ for an energy-driven flow. While the cooling time is greater than the dynamical time, an initially energy-driven flow can remain energy-driven. Thus, flows can remain energy driven if $\beta \leq -\frac{1}{2}$. If $0 > \beta > -\frac{1}{2}$, energy-driven flows can become momentum driven. An initially momentum-driven flow can only be maintained if $\beta > 0$, otherwise it becomes energy driven.

Main sequence stellar winds interacting with a uniform density ambient medium ($\beta = 0$) will normally be initially energy driven, unless the wind itself is very dense and can cool immediately once it shocks. The flow will remain energy driven because of the high postshock temperatures until, eventually, this gas begins to cool. If thermal conduction is important between the hot, shocked wind region and the cold swept-up shell, this can lower the temperature and raise the density in the hot bubble. This would enhance the cooling rate and so the changeover to a momentum-driven flow would occur earlier.

---

[1] The strong shock conditions $p = \frac{3}{4}\rho_R V_w^2$, $n = 4\rho_R/m_p$ and $T = \frac{3}{32}V_w^2 m_p/k$ have been used in the derivation.

A Wolf-Rayet star wind has a high mass-loss rate and could initially produce a momentum-driven flow. However, the density gradient of the red supergiant wind ($\beta = -2$) would quickly lead to a changeover to an energy-driven flow.

Observationally, it should be possible to discriminate between energy-driven and momentum-driven flows by determining the efficiency factors for the conversion of stellar wind mechanical energy and momentum into swept-up gas kinetic energy and momentum (Treffers & Chu, 1982). From the analytical model, an energy-driven flow has a kinetic energy efficiency factor $\epsilon = 3(5+\beta)/(11+\beta)(7+2\beta)$ and a momentum efficiency factor $\mu = \epsilon(V_w/V_s)$, while for a momentum-driven flow the corresponding values are $\epsilon = V_s/V_w$ and $\mu = 1$. Values of $\epsilon \ll 0.1$ are taken to indicate a momentum-driven flow. In practice, however, it is difficult to estimate ϵ since the masses of both neutral and ionized components must be taken into account (Dyson & Smith, 1985). Furthermore, outer shells may no longer be driven directly by the current stellar wind if the bubble has become depressurized.

Thermal conduction

Weaver et al. (1977) obtain a self-similar solution for the temperature structure across the hot bubble under the assumptions that the pressure is constant with radius and thermal conduction from the hot shocked wind to the cold swept-up shell is important. It is also assumed that radiative losses are negligible compared to the conductive and mechanical energy fluxes. In this model, the mass within the hot bubble is dominated by the evaporated mass from the shell, while this mass is negligible compared with that remaining in the shell. The self-similar solution for the temperature distribution across the hot bubble is

$$T(r) = T_b(1 - \frac{r}{R_s})^{2/5} , \qquad (14)$$

where $T_b = a\dot{E}_w^{8/35}n_0^{2/35}t^{-6/35}$ is the temperature in the inner part of the bubble and a is a constant which depends on the value of the conduction coefficient. This model has been extended to include the effect of expansion in a power-law density distribution and non-spherical (but uniform) expansion by García-Segura & Mac Low (1995a), but the same dependence on the similarity variable r/R_s is retained. It has been argued (e.g., Dyson, 1981) that thermal conduction will not, in fact, be important in stellar wind bubbles since the magnetic fields in the swept-up material will suppress it. It turns out that the temperature and density profiles predicted by the self-similar model of Weaver et al. (1977) significantly overestimate the X-ray emission, as compared to what has been observed, for a given set of stellar wind bubble parameters (Wrigge et al., 2005).

2 Numerical simulations of wind-blown bubbles

Numerical simulations are a powerful tool for studying the hydrodynamics of wind-blown bubbles, complementing analytical studies since many more physical processes can be included.[2] The first, spherically symmetric, numerical studies included radiative cooling and were able to follow the transition between the initial fully adiabatic stage to the stage where the swept-up interstellar medium cools radiatively (Falle, 1975). Subsequent numerical studies in two dimensions show that instabilities develop during the evolution of wind-blown bubbles, where the nature of the instability present depends on the evolutionary stage and physics being considered. Kelvin-Helmholtz, Rayleigh-Taylor, Richtmeyer-Meshkov, Vishniac, and thermal instabilities have all been reported (Rozyczka, 1985; Rozyczka & Tenorio-Tagle, 1985a,b; García-Segura & Mac Low, 1995b; García-Segura et al., 1996a,b; Brighenti & D'Ercole, 1995a,b, 1997; Strickland & Stevens, 1998; Freyer et al., 2003). However, care must be taken in the identification of these instabilities, since the resolution of the numerical grid can play an important role, as can parameters such as the cutoff temperature below which radiative cooling is assumed equal to zero (see Zhekov & Myasnikov, 2000b, for a more detailed discussion). Although the most widely used analytical models take into account thermal conduction (Weaver et al., 1977; García-Segura & Mac Low, 1995a), very few numerical studies include this process (notable exceptions are Zhekov & Myasnikov, 1998, 2000a,b). The presence of even a weak magnetic field will be enough to cause asymmetric thermal conduction and will thus lead to an asymmetric wind-blown bubble (Zhekov & Myasnikov, 2000b).

In this section, the evolution of a wind-blown bubble around a $40 M_\odot$ star from the main-sequence phase, through the red supergiant phase to the final Wolf-Rayet phase is examined by means of numerical simulations. The first two stages are treated as one-dimensional (spherically symmetric) simulations, while the start of the Wolf-Rayet phase is modelled in two dimensions (cylindrical symmetry). Photoionization is included using the method described in Henney et al. (2005). Radiative cooling and photoionization heating are also taken into account. Thermal conduction and magnetic fields are not included in these models. A simple three-wind model is considered, where the stellar wind mass-loss rate and velocity is taken to be constant during each phase and the ambient medium has uniform density and temperature (cf. García-Segura & Mac Low, 1995b; van Marle et al., 2005). Although a particular simulation is described here, the general features are common to all simulations of the evolution of wind-blown bubbles.
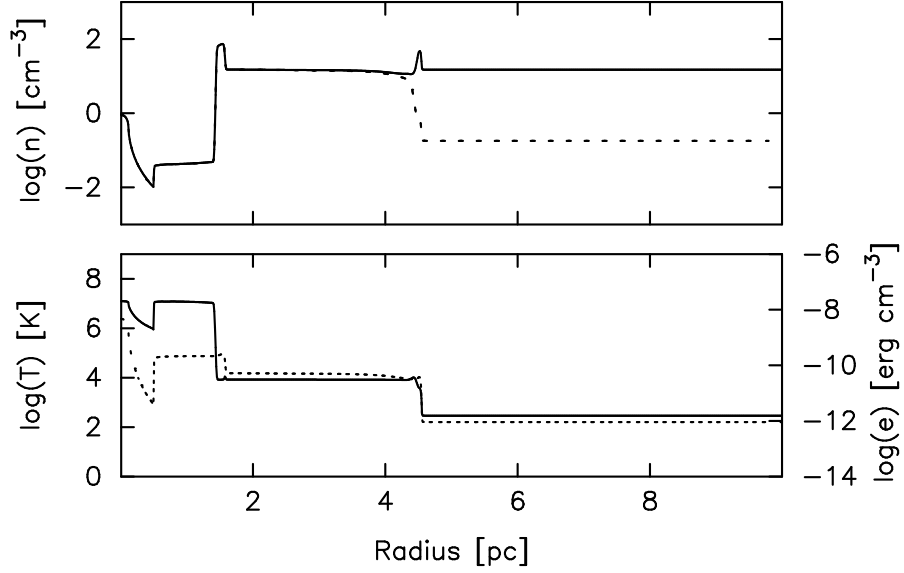
Fig. 2. Radial structure of a stellar wind bubble and H II region around a $40M_\odot$ star at an early stage of evolution (after 40,000 years). Top panel: total number density (solid line) and ionized number density (dotted line). Bottom panel: temperature (solid line) and internal energy ($e = p/[\gamma - 1]$ — dotted line). Stellar parameters $\dot{M}_w = 9.1 \times 10^{-7}M_\odot$ yr $^{-1}$, $V_w = 890$ km s^{-1}, and $S_* = 6.34 \times 10^{47}$ s^{-1} (adapted from van Marle et al., 2005).

2.1 Main sequence evolution

The main-sequence evolution of the ionized region (H II region) and stellar wind bubble around a $40M_\odot$ star in a uniform, neutral ambient medium with constant stellar wind and ionizing photon rate is presented here. The initial neutral ambient medium is taken to have density $n_{\rm H} = 15$ cm^{-3} and temperature 300 K, while the stellar wind has a mass-loss rate of $\dot{M}_w = 9.1 \times 10^{-7}M_\odot$ yr $^{-1}$ and wind terminal velocity $V_w = 890$ km s^{-1}, and the ionizing photon rate is $S_* = 6.34 \times 10^{47}$ s^{-1} (cf. Schaller et al., 1992; van Marle et al., 2005).[3]

The H II region forms immediately, reaching an initial Strömgren radius of ~ 4.5 pc. A low-velocity, isothermal shock forms ahead of the ionization front in the neutral gas and the hot ($T = 10^4$ K) ionized region begins to expand.

---

[2] Numerical simulations solve the full gas-dynamic equations and physical processes are generally included via source terms.

[3] In these simulations, the stellar wind is injected in the form of a thermal energy and mass source in a small volume around the star, and for this reason temperatures in the *unshocked* stellar wind region are high but do not affect the dynamics since the flow is highly supersonic in this region.

The stellar wind bubble forms inside this ionized region. Cooling in the swept up ionized gas is very efficient (see, e.g., Falle, 1975) and this region quickly forms a thin, dense shell. The increase in opacity traps the ionizing photons and the main ionization front becomes confined to this swept-up shell. The region between the shell and the outer isothermal shock is occupied by gas that belonged to the initial Strömgren sphere and is now slowly recombining (recombination time is approximately $10^5/n$ years). This can be seen in Figure 2, which shows the density, ionized density, temperature and thermal energy (i.e., pressure) structure after 40,000 years of evolution. The outer ionization front is no longer sharp since gas here has started to recombine. However, the shock that was launched ahead of the ionization front continues to expand at < 10 km s^{-1} into the neutral ambient medium.

In two-dimensional simulations, strong radiative cooling in the swept-up ambient medium leads to the formation of instabilities, which cause corrugation of the shell (Strickland & Stevens, 1998; Freyer et al., 2003). Shadowed regions then form in the H II region beyond the stellar wind shell and recombination occurs faster here, leading to a pattern of neutral spokes and non-radial velocity fields (Freyer et al., 2003; Arthur & Hoare, 2005).

Eventually, the wind bubble overtakes the outer neutral shock. By this time, the swept-up shell of material has spread out and its density has dropped. This is because the pressure in the shell is the same as that in the hot wind bubble, which falls slowly as the inner wind shock moves outwards. Since the temperature in the swept-up shell is determined by photoionization, and is thus a constant $\sim 10^4$ K, then the density has to fall (and hence the swept-up shell must broaden) to account for the fall in pressure. The inner wind shock will continue to move outwards until the ram pressure of the stellar wind here ($\rho_w V_w^2 \equiv \dot{M}_w V_w/4\pi R_s^2$) balances the pressure of the interstellar medium. The H II region establishes itself in this, now, low-density shell, and sends a shock ahead into the neutral gas.

Figure 3 shows the radial structure of the stellar wind bubble and H II region at the end of the main sequence stage, after some 4.31×10^6 years of evolution. The inner stellar wind shock is located about 3 pc from the star. The hot ($T \sim 10^7$ K), very low density ($n_i \sim 10^{-3}$ cm^{-3}) shocked stellar wind bubble occupies the region $3 < R < 24.5$ pc. Outside of this is the shell containing the H II region. The ionized gas has density $n_i \sim 1$ cm^{-3} and temperature $T = 10^4$ K, and extends between $24.5 < R < 27.5$ pc. The broad neutral shell, $27.5 < R < 33.5$ pc, has density $n_n \sim 30$ cm^{-3} and temperature $T \sim 10^3$ K. The entire region between $3 < R < 33.5$ pc has uniform pressure and is still expanding slowly into the ambient medium.

2.2 Post-main-sequence evolution

In Figure 4, the possible mass loss history of a $60 M_\odot$ star is shown (Langer et al., 1994; García-Segura et al., 1996a). A detailed study of the evolution of the wind-blown bubble around stars of initial masses 60 $M_\odot$ and 35 $M_\odot$ has been
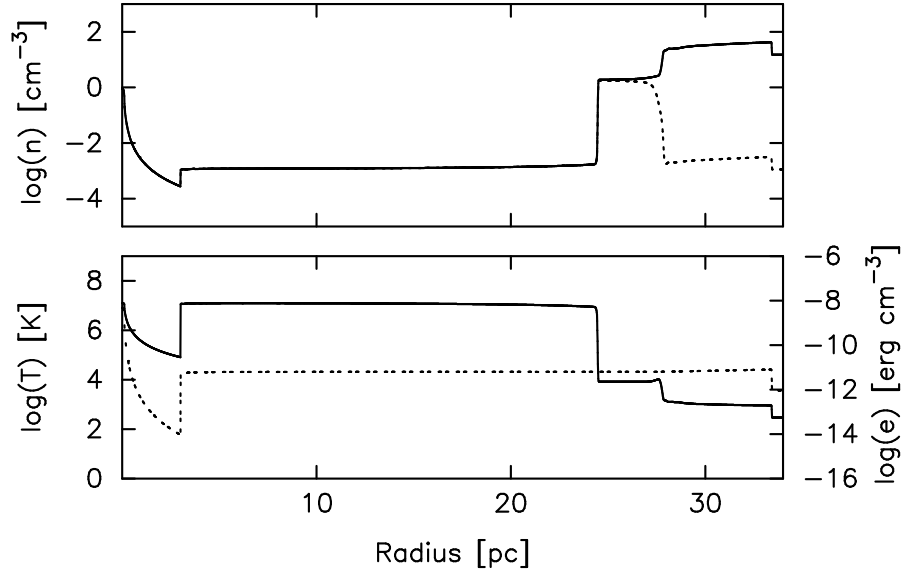
Fig. 3. Radial density and temperature structure of the stellar wind bubble around a $40 M_\odot$ star at the end of the main sequence stage, i.e. after $\sim 4.3 \times 10^6$ years. Line types are the same as for Fig. 2.
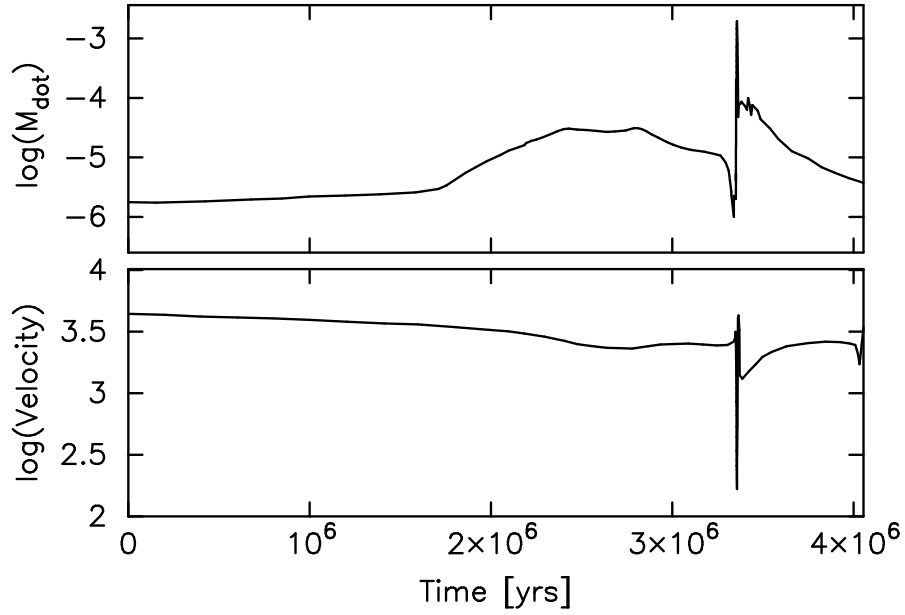

Fig. 4. Variation of mass-loss rate $(M_\odot \ \mathrm{yr}^{-1})$ and stellar wind velocity $(\mathrm{km \ s}^{-1})$ as a function of time for a $60 M_\odot$ star (data from García-Segura et al., 1996a).

carried out by García-Segura et al. (1996a,b), for the purely hydrodynamic case, and by Freyer et al. (2003, 2005), including the radiative transfer of ionizing photons. The numerical simulations predict short-lived, observable nebulae during the LBV or RSG stage and the onset of the WR stage. Instabilities are formed in the dense shells swept-up by the different stellar wind stages, and these are consistent with clumps observed in ring nebulae around some Wolf-Rayet stars. The velocity of the LBV or RSG wind is found to play a key role in the detailed structure of the ring nebulae formed during this process.
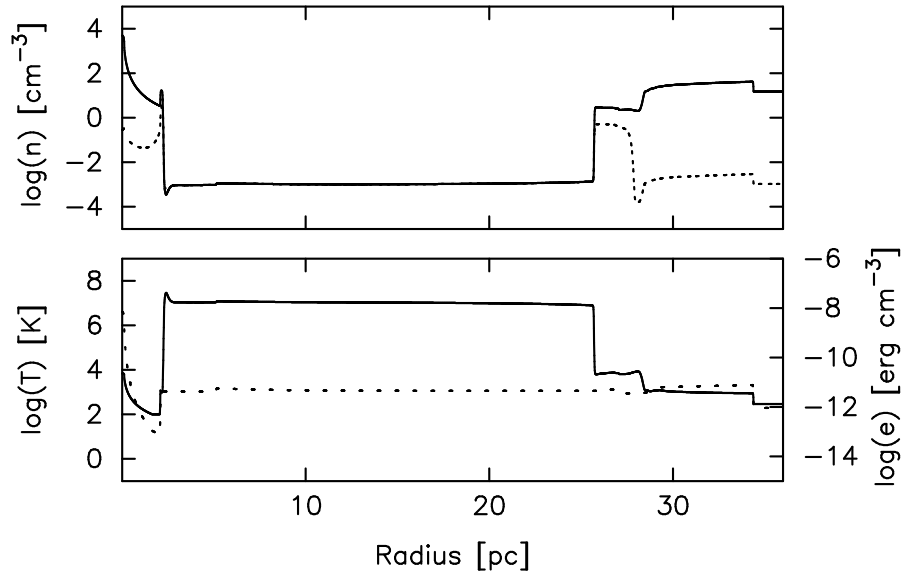
Red supergiant phase

Fig. 5. Radial structure of a stellar wind bubble around a 40 $M_\odot$ star at the end of the red supergiant stage, i.e. after 4.5×10^6 years. Top panel: total number density (solid line) and ionized number density (dotted line). Bottom panel: temperature (solid line) and internal energy ($e = p/[\gamma - 1]$ — dotted line).

During the red supergiant (RSG) phase, the ionizing photon luminosity of the 40 $M_\odot$ star drops to 3.1×10^{41} photons s^{-1}, and the stellar wind velocity drops to 15 km s^{-1} while the mass-loss rate increases to 8.3×10^{-5} $M_\odot$ yr^{-1} (van Marle et al., 2005). This phase lasts only 2×10^5 years (an LBV phase would have an even higher mass-loss rate but a much shorter timescale, see Fig. 4). The slow, dense RSG wind expands into the structure formed by the main sequence wind and a thin, dense shell of shocked RSG material forms

ahead of the freely expanding wind (see Figure 5). The high thermal pressure in the hot main sequence bubble causes backflow of low-density gas towards the star, which shocks against the RSG wind. The reduction in the ionizing photon rate leads to the disappearance of the H II region as the shell of ionized gas recombines. The hot bubble remains ionized since the recombination times are long in this hot, very low-density gas. The RSG wind itself is neutral.
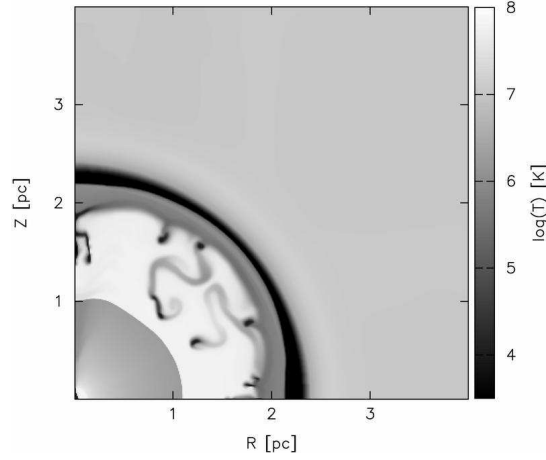
Wolf-Rayet phase

Fig. 6. Formation of Rayleigh-Taylor instabilities in the Wolf-Rayet wind shell just before the interaction with the red supergiant shell. The instabilities form as the WR wind accelerates into the r^{-2} density distribution left by the RSG wind. The temperature of the gas is shown 8000 years after the start of the Wolf-Rayet wind. Only one quadrant is shown, and the star is located at $(0,0)$.

The Wolf-Rayet wind expands into the structure formed during the previous two phases. During the Wolf-Rayet phase, the stellar wind becomes faster ($V_w = 2160$ km s^{-1}) and remains strong ($\dot{M}_w = 4.1 \times 10^{-5}$ $M_\odot$ yrs^{-1}) and the stellar ionizing photon rate also increases ($S_* = 3.86 \times 10^{47}$ s^{-1}). The transition between the RSG and WR winds will involve a period of wind acceleration into the r^{-2} density distribution left by the RSG wind, and this situation is Rayleigh-Taylor unstable.[4] The WR shell consists of swept-up RSG wind material and shocked WR wind. It becomes Rayleigh-Taylor unstable at an early time in the simulation, well before the interaction with the RSG shell. Dense, cold clumps of material formed by the instability lag behind

---

[4] In the numerical simulations presented here, acceleration of the wind occurs initially as a consequence of the way in which the stellar wind is included in the calculation.

the main WR shell but the shell itself is not disrupted, since the instabilities cease to grow once the acceleration stage is over (see Fig. 6).
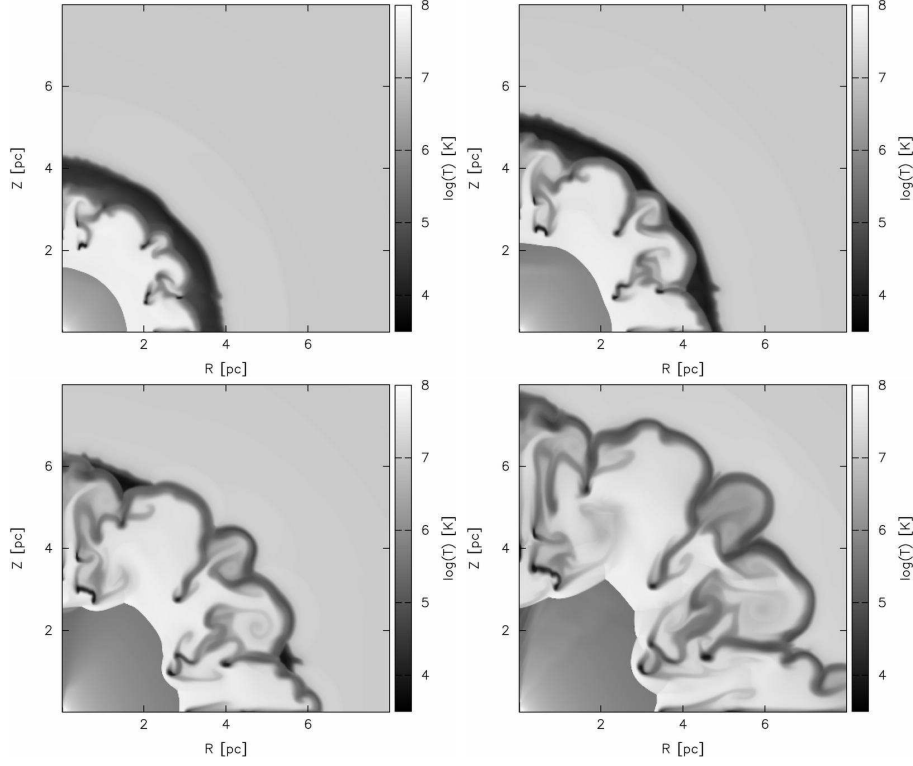
Fig. 7. Interaction of the Wolf-Rayet wind with the dense shell from the red super-giant stage. Rayleigh-Taylor instabilities form as the WR wind accelerates into the r^{-2} density distribution left by the RSG wind. The instabilities become enhanced when the WR wind collides with the dense RSG shell and ruptures it. The panels show the temperature of the gas after times (a) 15,000 years, (b) 18,000 years (c) 21,000 years and (d) 24,000 years after the start of the WR wind.

Figure 7 shows the evolutionary sequence of the interaction of the WR shell with the RSG shell. The dense, cold clumps formed due to Rayleigh-Taylor instabilities in the WR shell act as obstacles around which the hot, shocked WR wind has to flow. Large amplitude ripples form in the RSG shell, through which the WR wind eventually breaks out into the low-density bubble formed by the main-sequence wind. The dense, cold clumps formed by the Rayleigh-Taylor instabilities move outwards more slowly. These clumps will be subject to hydrodynamic and photoablation but the numerical resolution of the two-dimensional simulation is not able to follow these processes. The

mixing process produces gas with temperatures $\sim 10^6$ K, which should emit X-rays.

During the red supergiant phase, 16.5 $M_\odot$ of material are lost from the star. All of this material is swept into clumps and filaments by the Wolf-Rayet wind, which are potential *mass-loading* sources of the WR wind, to be discussed later.
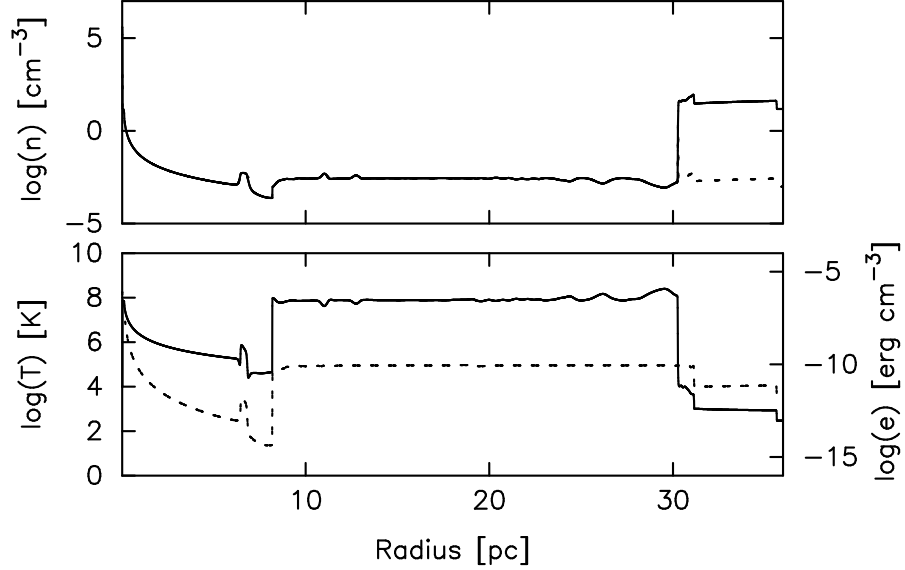

Fig. 8. Radial structure of a stellar wind bubble around a 40 $M_\odot$ star at the end of the Wolf-Rayet phase, i.e. after a total time of 4.8×10^6 years. Top panel: total number density (solid line) and ionized number density (dotted line). Bottom panel: temperature (solid line) and internal energy ($e = p/[\gamma - 1]$ — dotted line).

Figure 8 shows the final radial structure of the wind bubble around the $40 M_\odot$ star just before it explodes as a supernova, from a one-dimensional (spherical symmetry) numerical simulation. The low-density bubble has been repressurized by the hot, shocked WR wind material, a new shock is being driven into the neutral shell, and the H II region is starting to reform. The one-dimensional simulation cannot show the fate of the clumps and filaments formed during the initial interaction between the WR wind and the RSG shell.

2.3 Energy evolution in a wind-blown bubble

Figure 9 shows the evolution of the neutral and ionized gas kinetic and thermal energy fractions with respect to the total stellar wind mechanical energy, $\dot{E}_w t$, resulting from the numerical simulations described above. During the main
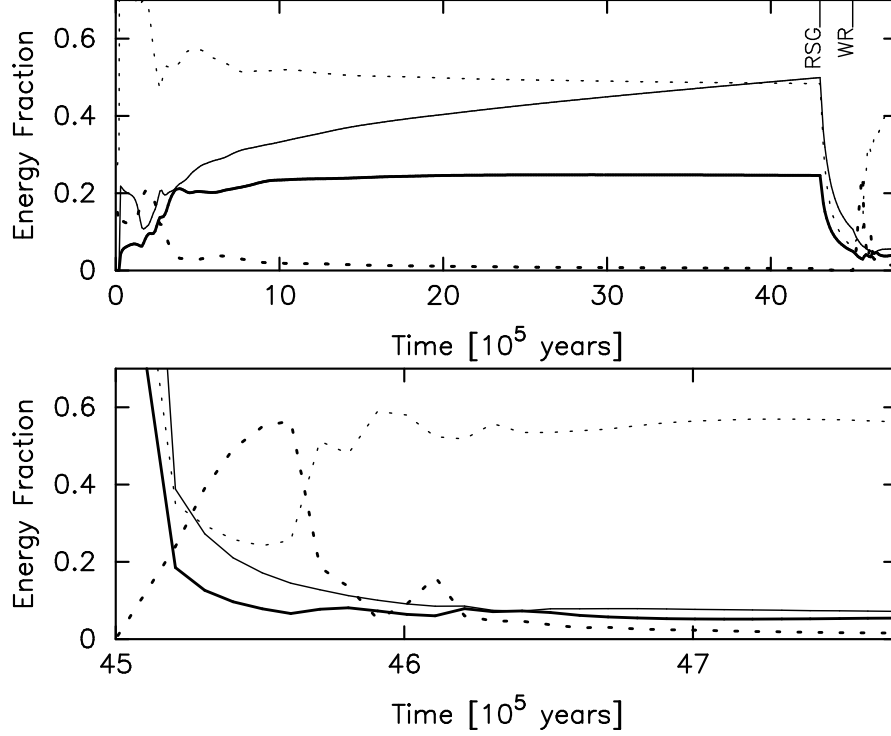
Fig. 9. Top panel: Kinetic and thermal energies of the ionized and neutral gas as fractions of the total stellar wind mechanical energy as a function of time for the numerical simulation described in this paper. Thick lines represent kinetic energy and thin lines represent thermal energy, while solid lines represent neutral gas and dotted lines represent ionized gas energy fractions. The onset of the RSG and WR are indicated. Bottom panel: Kinetic and thermal energies as fractions of the WR stellar wind mechanical energy, $\dot{E}_w(t - t_{\mathrm{WR}})$ during the WR phase.

sequence stage, the initial 400,000 yrs show large variations in the relative importance of the kinetic energies in the neutral and ionized gas. This is because this period of time sees the formation and expansion of the initial H II region, which then retreats back into the shell of material swept up by the stellar wind before expanding outwards again driven by the pressure in the hot bubble. The majority of the main-sequence stage sees an energy-driven bubble in which the thermal energy of the hot bubble pushes the expansion of a neutral shell of material. The kinetic energy of the swept-up neutral shell is roughly 0.25 of the stellar wind mechanical energy for most of this stage. This is larger than the fraction $\frac{15}{77}$ predicted by the simple thin-shell model (see e.g., Dyson & Williams, 1997) and can be attributed to the H II region. It is the H II region that results in the different fractions summing to more than unity, since the contribution to the thermal energy by the heating of the H II

region in the shell surrounding the low-density bubble is substantial (see also Freyer et al., 2003). Observations of only the ionized gas during this phase would show $\epsilon \ll 0.1$, suggesting a momentum-driven flow, while observations of the neutral shell would give $\epsilon > 0.1$, hence an energy-driven flow.

When the red supergiant phase begins, the ionizing photons are trapped close to the star and the outer H II region recombines. Also, the driving pressure in the hot bubble drops because the RSG stellar wind is such low velocity. As a result, both the thermal and kinetic energy fractions drop. Observations of both neutral and ionized gas during this phase would give $\epsilon < 0.1$, suggesting a momentum-driven flow.

During the Wolf-Rayet phase, the RSG wind material is ionized by the high flux of ionizing photons and the high velocity WR wind forms a hot, high-pressure bubble. This is reflected in the energy fractions of the ionized gas, which rise steeply during this phase. It is a long time before the wind-blown bubble becomes pressurized out to the neutral shell, and so the neutral gas thermal and kinetic energy fractions remain low. Observations of the ionized gas during this stage would show $\epsilon > 0.1$ initially, but later in the evolution $\epsilon \ll 0.1$ even though the flow is now energy driven. The neutral gas kinetic energy fraction corresponds to the outer swept-up shell, which is not repressurized or accelerated during the timescale we are considering. Consequently, observations of the neutral shell during this stage of evolution would indicate that $\epsilon < 0.1$.

Figure 9 shows that neither observations of only the ionized gas or only the neutral gas can reveal the full picture of the energetics of a wind-blown bubble. Observations of the outer neutral shell during this stage do not provide a true picture of what is happening with the interaction between the current stellar wind and its surroundings.

2.4 Mass loading

The presence of dense clumps embedded in a fast flowing stellar wind and subject to a large flux of ionizing photons from the central star suggests the possibility that material from the clumps will be incorporated into the flow by one or other mass-loading processes, namely photoevaporation, conductive evaporation or hydrodynamic ablation. If the amount of mass incorporated into the flow becomes important then the dynamics of the flow can be radically altered. Both supersonic and subsonic flows tend to an average transonic flow, and the positions of global shock waves change (Smith, 1996). Furthermore, if the mass loading is strong enough, the density in the hot shocked stellar wind can increase sufficiently that cooling becomes important in this region.

Mass loading by embedded clumps in a stellar wind was first proposed to explain the ionization potential-velocity correlation observed in the WR ring nebula RCW 58 (Smith et al., 1984; Hartquist et al., 1986). In this scenario, the mass-loading is due to hydrodynamic ablation and has two regimes: one

in which the flow around the clump is subsonic and the other when it is supersonic. In the subsonic case, the mass-loading rate is proportional to $M^{4/3}$, where M is the flow Mach number. In the supersonic case, the mass-loading rate saturates and is taken to be constant. Numerical modelling of the mass-loaded flow in RCW 58 shows that the position of the stellar wind shock is fixed by the mass loading and that cooling occurs in the outer parts of the hot shocked bubble (Arthur et al., 1993, 1996).

3 Observations of wind-blown bubbles

Bubbles around massive stars can be detected in a variety of ways: as optical ring-shaped nebulae (e.g., Chu, 1981), as shell-shaped thermal radio continuum sources (e.g., Goss & Lozinskaya, 1995), as neutral gas voids and expanding shells in the hydrogen 21 cm line-emission distribution (Cappa et al., 2005), as infrared shells (e.g., Marston, 1996), and in a limited number of cases as diffuse X-ray sources (e.g., Wrigge, 1999). Gamma-ray burst afterglows probe the innermost regions of the progenitor wind bubble (Chevalier et al., 2004), and Type II and Type Ib/c supernova narrow spectral absorption features can be attributed to moving shells around the massive star progenitor (Dopita et al., 1984).

Multiple concentric shells of material have been observed around many galactic WR stars (Marston, 1996).[5] The outermost shells are thought to correspond to the O star phase, and are most readily observable at far infrared or 21 cm radio wavelengths, although around 8% are seen optically. These outer shells have can very large diameters (> 100 pc), depending on the ambient ISM density, and are expanding slowly (generally, $v_{\exp} < 10$ km s^{-1} Marston, 1996). The innermost shells are easily seen in optical narrowband images, and represent dense material recently ejected from the star in a LBV or RSG phase or swept up by the stellar wind in the WR phase.

Of the ~ 150 observed Galactic WR stars about 25% are associated with optical ring-like nebulae (Heckathorn et al., 1982; Chu et al., 1983; Miller & Chu, 1993; Marston et al., 1994a,b). However, only ~ 10 of these WR ring nebulae have the sharp rims and short dynamical ages (ring radius divided by expansion velocity) that suggest that they are bubbles formed by the winds of the central stars during the WR phase.[6] The remaining ring nebulae are

---

[5] Ring nebulae have also been observed around WR stars in the Large Magellanic Cloud (Dopita et al., 1994) but their distance makes them less easy to study.

[6] These objects are: S 308, RCW 58, RCW 104, NGC 2359, NGC 3199, NGC 6888, Anon (MR26), G2.4+1.4, and there is kinematical evidence that the nebulae around WR 116 and WR 133 have expansion velocities consistent with wind-blown bubbles (Esteban & Rosado, 1995). Anon(WR 128) and Anon(WR 134) are possibly wind-blown bubbles, too (Gruendl et al., 2000). There are also wind-blown bubbles around two other evolved stars: NGC 6164-5 (around an O6.5fp star), NGC 7635 (around an O6.5III star).

less well defined and have dynamical ages much larger than the lifetime of a WR phase, and hence are thought to be simply stellar ejecta from the RSG or LBV stage photoionized by the WR star (like a planetary nebula), rather than dynamically shaped by its wind. Wind-blown bubbles were established as a class of object by Chu (1981) and Lozinskaya (1982).
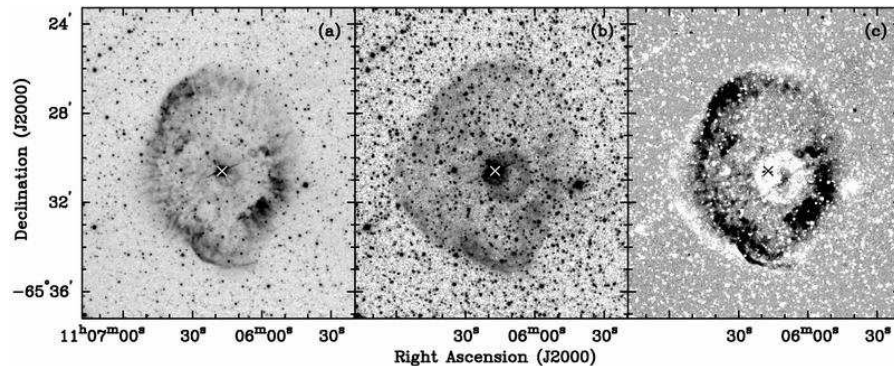

Fig. 10. (a) Optical Hα and (b) [O III] λ5007 images of the ring nebula RCW 58, together with (c) an image of their difference (Gruendl et al., 2000).

A striking example of an optical WR ring nebula is RCW 58 (see Figure 10). This nebula consists of clumps and filaments extending radially outward from the central WN8 star, seen in Hα, with more diffuse [O III] emission extending beyond (Chu, 1982; Gruendl et al., 2000). The nebula is enriched in He and N, which indicates that the material has been ejected from the star, probably during a red supergiant stage. The expansion velocity of the shell is 87 km s^{-1}, and broad linewidths indicate supersonic motions (Smith et al., 1988). The measured electron densities of the clumps are ∼500 cm^{-3}.

Most WR wind-blown bubbles are aspherical to a lesser (e.g., RCW 58, S 308, NGC 6888) or greater (e.g., NGC 2359, NGC 3199, G2.4+1.4) degree. The asphericity is often more pronounced in Hα images than in [O III], suggesting that it arises in the RSG or LBV ejecta phase. Such morphologies could also be due to the environment: for example, NGC 2359 and NGC 3199 are each bounded on one side by molecular clouds (Schneps et al., 1981; Marston, 2001) and their roughly parabolic shapes in Hα images could be the result of the wind-bubble blowing out from near the surface of the dense cloud and expanding down a strong density gradient, as has been suggested in the case of G2.4+1.4 (Dopita & Lozinskaya, 1990). An alternative explanation for this sort of morphology could be that the star is moving supersonically through the ambient medium and forms a bowshock ahead of it (this was suggested as an explanation for G2.4+1.4 by Brighenti & D'Ercole, 1995b).

Four of the 8 WR wind-blown bubbles have been observed with X-ray satellites but only two of these, NGC 6888 and S 308, have been detected in
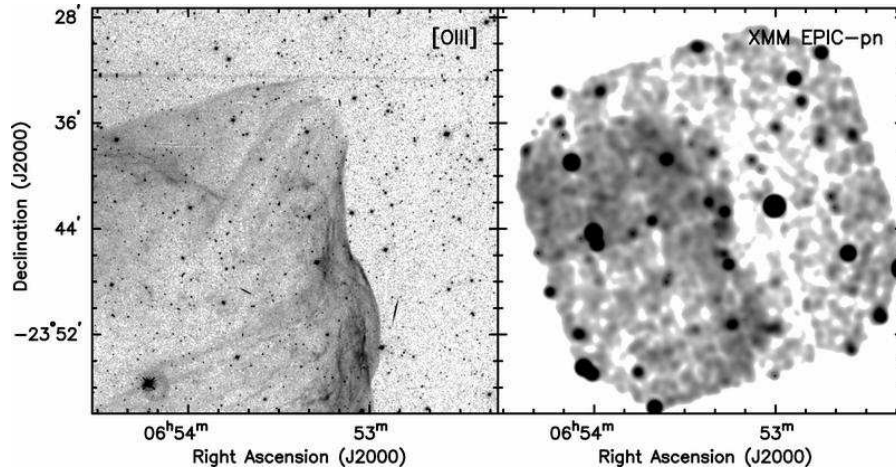
Fig. 11. Optical [O III] $\lambda5007$ image (left) and *XMM-Newton* EPIC image (right) of the northwest quadrant of S 308 (Chu et al. (2003); figure reproduced with permission from *Revista Mexicana de Astrononomía y Astrofísica*).

diffuse X-rays. Both were detected with the *ROSAT* PSPC in the energy range 0.1–2.4 keV and spectral analysis shows that the hot gas in these bubbles is dominated by the component at $\sim 1.5 \times 10^6$ K (Bochkarev, 1988; Wrigge et al., 1994; Wrigge, 1999), although this could be partially contaminated by higher energy point source emission. *ASCA* SIS observations of NGC 6888 suggests that there is an additional component of hot gas at a temperature of 8×10^6 K (Wrigge et al., 1998, 2005), while *XMM-Newton* EPIC observations of S 308 indicate that the spectrum is very soft, suggesting plasma temperatures of only 1×10^6 K (Chu et al., 2003). Figures 11 and 12 show the optical [O III] $\lambda5007$ and X-ray images of S 308 and NGC 6888, taken from Chu et al. (2003). The S 308 images clearly show that the X-ray emission is limb-brightened, and NGC 6888 appears to be limb-brightened also.[7] In both cases the X-ray emission is interior to the [O III] emission, which marks the position of the main shock wave.

4 Observations confront theory

It has been proposed that nebulae around massive stars begin with wind-blown shells in the main-sequence stage, evolve into amorphous H II regions, then ringlike H II regions, then nebulae with stellar ejecta in the RSG or LBV phase before the star explodes as a supernova (McKee et al., 1984). The bubbles blown by WR winds occur within the circumstellar material of the

---

[7] Although not clear from the *ROSAT* image, this is evident in recent *Chandra* images: http://www.chandra.harvard.edu/photo/2003/ngc6888.
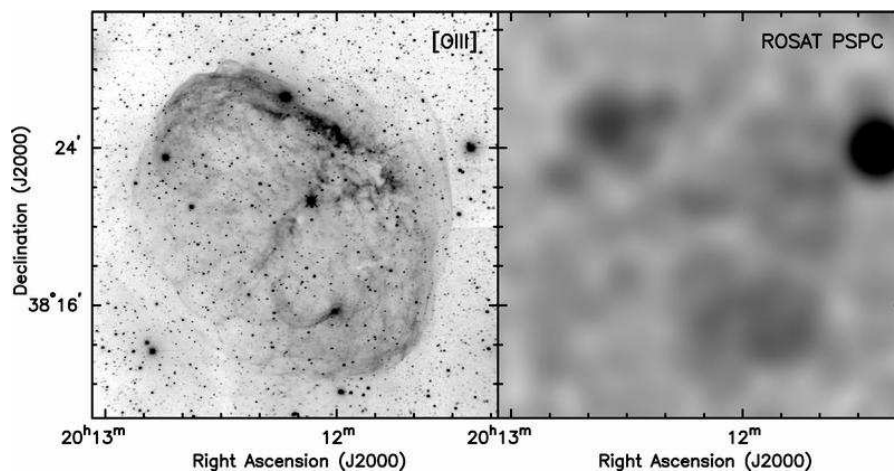
Fig. 12. Optical [O III] $\lambda5007$ image (left) and *ROSAT* PSPC image (right) of NGC 6888 (Chu et al., 2003, figure reproduced with permission from *Revista Mexicana de Astronomía y Astrofísica*).

RSG/LBV phase. In practise, wind-blown bubbles have rarely been observed around main-sequence O stars (although kinematic evidence suggests that wind-blown bubbles do exist inside H II regions Nazé et al., 2001). Ringlike H II regions may be too faint to observe but expanding HI shells with masses up to $10^4 M_\odot$ should occur around massive stars, as illustrated in Figure 3. In the later stages of massive star evolution and, indeed, around some supernova remnants, expanding HI shells are detected (Cappa et al., 2005) that must have originated in the main-sequence stage.

The fact that so few of the known WR stars are surrounded by wind-blown bubbles suggests that this is a short-lived phase of evolution (Chu, 1981). This is borne out by numerical simulations, which predict observable bubbles only during the early interaction of the WR wind with the LBV or RSG nebula (Freyer et al., 2003, 2005). More common are amorphous nebulae, which are observed around many WR stars, indicating a photoionization rather than wind-blown origin, even when there are clear indications that the central star possesses a strong stellar wind. These cases could be the result of the environment in which the nebula is found: if a strong density gradient is present the stellar wind will blow out in the direction of decreasing density rather than form a pressure-driven expanding bubble (Arthur & Hoare, 2005, discuss similar models in the context of cometary H II regions). Clumps and filaments observed in nebulae such as RCW 58 are formed naturally in numerical simulations by Rayleigh-Taylor and other instabilities (García-Segura et al., 1996a,b).

Theoretical estimates of X-ray emission as predicted by analytic theory fail to match the reality. Models that do not include thermal conduction

have very high temperatures in the shocked stellar wind and do not produce the soft X-ray spectrum that has been detected in NGC 6888 and S 308. On the other hand, the self-similar models of Weaver et al. (1977) and García-Segura & Mac Low (1995a), which include thermal conduction, predict much higher values of the soft X-ray luminosities than are observed. It appears that some sort of dissipative process, though not the classical thermal conduction proposed by Weaver et al. (1977), is necessary to produce the soft X-rays. This argument presupposes that the X-ray emission is produced in the shocked Wolf-Rayet wind material. Two-dimensional numerical simulations of the wind-blown bubble produced by a $35 M_\odot$ star Freyer et al. (2005), on the other hand, show that the X-ray emission actually arises in the shocked, dense RSG wind material. This can be appreciated in Figure 7, where gas temperatures of $\sim 10^6$ K, characteristic of soft X-rays are present in the shocked RSG shell material. Also, it could be expected that material photoevaporated or ablated from the dense clumps formed by the instabilities could augment the soft X-ray luminosity in the interaction region.

5 Final Remarks

Although the general characteristics of the formation and evolution of wind-blown bubbles around evolved stars are well understood, there remain a number of important features to explain. Most obviously, it is interesting to know whether the asphericity of nebulae such as NGC 6888 and RCW 58 is due to the non-spherical ejection of material in the RSG or LBV stage, or whether it is due to some direction-dependent physical process, such as thermal conduction, in the WR bubble phase. Photoionization is clearly important for the thermal balance and energetics of wind-blown bubbles and should not be neglected in numerical calculations. The role of instabilities in producing the clumps and filaments observed in some (but not all) bubbles should be examined in more detail. Cooling within the clumps can lead to the formation of very dense, neutral structures within the hot, ionized bubble. The ablation, either by photoevaporation, thermal conduction or hydrodynamic ablation, of this neutral material will modify the physical properties and chemical abundances of the hot, shocked wind and such processes should, therefore, be studied further. Theories should be tested with real data and new observations will always be needed, at all wavelengths, to provide more detailed kinematical information, abundance data, and improved stellar wind parameters.

References

Arthur, S. J., Dyson, J. E., & Hartquist, T. W. 1993, MNRAS, 261, 425
Arthur, S. J., Henney, W. J., & Dyson, J. E. 1996, A&A, 313, 897

Arthur, S. J., & Hoare, M. G. 2005, ArXiv Astrophysics e-prints, arXiv:astro-ph/0511035

Avedisova, V. S. 1972, Soviet Astronomy, 15, 708

Bochkarev, N. G. 1988, Nature, 332, 518

Brighenti, F., & D'Ercole, A. 1995a, MNRAS, 277, 53

Brighenti, F., & D'Ercole, A. 1995b, MNRAS, 273, 443

Brighenti, F., & D'Ercole, A. 1997, MNRAS, 285, 387

Cappa, C., Niemela, V. S., Martín, M. C., & McClure-Griffiths, N. M. 2005, A&A, 436, 155

Chevalier, R. A., Li, Z.-Y., & Fransson, C. 2004, ApJ, 606, 369

Chu, Y.-H. 1981, ApJ, 249, 195

Chu, Y.-H. 1982, ApJ, 254, 578

Chu, Y.-H., Gruendl, R. A., & Guerrero, M. A. 2003, Revista Mexicana de Astronomia y Astrofisica Conference Series, 15, 62

Chu, Y.-H., Guerrero, M. A., Gruendl, R. A., García-Segura, G., & Wendker, H. J. 2003, ApJ, 599, 1189

Chu, Y.-H., Treffers, R. R., & Kwitter, K. B. 1983, ApJS, 53, 937

Dopita, M. A., Cohen, M., Schwartz, R. D., & Evans, R. 1984, ApJ, 287, L69

Dopita, M. A., & Lozinskaya, T. A. 1990, ApJ, 359, 419

Dopita, M. A., Bell, J. F., Chu, Y.-H., & Lozinskaya, T. A. 1994, ApJS, 93, 455

Dyson, J. E. 1981, ASSL Vol. 91: Investigating the Universe, 125

Dyson, J. E. 1984, Ap&SS, 106, 181

Dyson, J. E. 1989, LNP Vol. 350: IAU Colloq. 120: Structure and Dynamics of the Interstellar Medium, 350, 137

Dyson, J. E., & de Vries, J. 1972, A&A, 20, 223

Dyson, J. E., & Smith, L. J. 1985, Cosmical Gas Dynamics, 173

Dyson, J. E., & Williams, D. A. 1997, The physics of the interstellar medium. Edition: 2nd ed. Publisher: Bristol: Institute of Physics Publishing, 1997. Edited by J. E. Dyson and D. A. Williams. Series: The graduate series in astronomy. ISBN: 0750303069,

Esteban, C., & Rosado, M. 1995, A&A, 304, 491

Falle, S. A. E. G. 1975, A&A, 43, 323

Freyer, T., Hensler, G., & Yorke, H. W. 2003, ApJ, 594, 888

Freyer, T., Hensler, G., & Yorke, H. W. 2005, ArXiv Astrophysics e-prints, arXiv:astro-ph/0512110

García-Segura, G., & Mac Low, M.-M. 1995a, ApJ, 455, 145

García-Segura, G., & Mac Low, M.-M. 1995b, ApJ, 455, 160

García-Segura, G., Mac Low, M.-M., & Langer, N. 1996a, A&A, 305, 229

García-Segura, G., Langer, N., & Mac Low, M.-M. 1996b, A&A, 316, 133

Goss, W. M., & Lozinskaya, T. A. 1995, ApJ, 439, 637

Gruendl, R. A., Chu, Y.-H., Dunne, B. C., & Points, S. D. 2000, AJ, 120, 2670

Hartquist, T. W., Dyson, J. E., Pettini, M., & Smith, L. J. 1986, MNRAS, 221, 715

Heckathorn, J. N., Bruhweiler, F. C., & Gull, T. R. 1982, ApJ, 252, 230

Henney, W. J., Arthur, S. J., & García-Díaz, M. T. 2005, ApJ, 627, 813

Kahn, F. D. 1976, A&A, 50, 145

Langer, N., Hamann, W.-R., Lennon, M., Najarro, F., Pauldrach, A. W. A., & Puls, J. 1994, A&A, 290, 819

Lozinskaya, T. A. 1982, Ap&SS, 87, 313

Marston, A. P., Chu, Y.-H., & García-Segura, G. 1994a, ApJS, 93, 229

Marston, A. P., Yocum, D. R., García-Segura, G., & Chu, Y.-H. 1994b, ApJS, 95, 151

Marston, A. P. 1996, AJ, 112, 2828

Marston, A. P. 2001, ApJ, 563, 875

McKee, C. F., van Buren, D., & Lazareff, B. 1984, ApJ, 278, L115

Miller, G. J., & Chu, Y.-H. 1993, ApJS, 85, 137

Nazé, Y., Chu, Y.-H., Points, S. D., Danforth, C. W., Rosado, M., & Chen, C.-H. R. 2001, AJ, 122, 921

Pikel'ner, S. B. 1968, Astrophysical Letters, 2, 97

Rozyczka, M. 1985, A&A, 143, 59

Rozyczka, M., & Tenorio-Tagle, G. 1985a, A&A, 147, 202

Rozyczka, M., & Tenorio-Tagle, G. 1985b, A&A, 147, 209

Schaller, G., Schaerer, D., Meynet, G., & Maeder, A. 1992, A&AS, 96, 269

Schneps, M. H., Haschick, A. D., Wright, E. L., & Barrett, A. H. 1981, ApJ, 243, 184

Smith, S. J. 1996, ApJ, 473, 773

Smith, L. J., Pettini, M., Dyson, J. E., & Hartquist, T. W. 1984, MNRAS, 211, 679

Smith, L. J., Pettini, M., Dyson, J. E., & Hartquist, T. W. 1988, MNRAS, 234, 625

Strickland, D. K., & Stevens, I. R. 1998, MNRAS, 297, 747

Treffers, R. R., & Chu, Y.-H. 1982, ApJ, 254, 569

van Marle, A. J., Langer, N., & García-Segura, G. 2005, A&A, 444, 837

Weaver, R., McCray, R., Castor, J., Shapiro, P., & Moore, R. 1977, ApJ, 218, 377

Wrigge, M., Wendker, H. J., & Wisotzki, L. 1994, A&A, 286, 219

Wrigge, M. 1999, A&A, 343, 599

Wrigge, M., Chu, Y.-H., Magnier, E. A., & Kamata, Y. 1998, LNP Vol. 506: IAU Colloq. 166: The Local Bubble and Beyond, 506, 425

Wrigge, M., Chu, Y.-H., Magnier, E. A., & Wendker, H. J. 2005, ApJ, 633, 248

Wrigge, M., & Wendker, H. J. 2002, A&A, 391, 287

Zhekov, S. A., & Myasnikov, A. V. 1998, New Astronomy, 3, 57

Zhekov, S. A., & Myasnikov, A. V. 2000a, ApJ, 543, L53

Zhekov, S. A., & Myasnikov, A. V. 2000b, Ap&SS, 274, 243